Broadband sensitivity enhancement of detuned dual-recycled Michelson interferometers with EPR entanglement

Daniel D. Brown,[*] Haixing Miao, Chris Collins, Conor Mow-Lowry, Daniel Töyrä, and Andreas Freise[†]

School of Physics and Astronomy and Institute of Gravitational Wave Astronomy,
University of Birmingham, Edgbaston, Birmingham B15 2TT, United Kingdom
(Received 25 April 2017; published 14 September 2017)

We demonstrate the applicability of the EPR entanglement squeezing scheme for enhancing the shot-noise-limited sensitivity of detuned dual-recycled Michelson interferometers. In particular, this scheme is applied to the GEO600 interferometer. The effect of losses throughout the interferometer, arm length asymmetries, and imperfect separation of the signal and idler beams is considered.

I. INTRODUCTION

Current and future generations of gravitational wave detectors will inject squeezed light to improve the quantum noise limited regions of their sensitivity [1,2]. Envisaged upgrades of gravitational wave detectors with a squeezed light source [3] will require external *filter cavities* [4,5] to provide a broadband reduction in the quantum noise. These filter cavities rotate the squeezed state to provide amplitude squeezing at low frequencies to reduce radiation pressure fluctuations and phase squeezing at higher frequencies to reduce shot noise. It has recently been proposed that a broadband reduction of quantum noise in gravitational wave detectors can be achieved using a pair of squeezed EPR-entangled beams to produce frequency-dependent squeezing [6]. This method promises to achieve a frequency-dependent optimization of the injected squeezed light fields without the need for an external filter cavity. Although suitable filter cavities can be designed, the additional cavity adds further complexity to the interferometer. *EPR squeezing* offers an attractive solution to this by harnessing the quantum correlations generated between a pair of EPR entangled beams [7–10] and effectively utilizing the interferometer itself as a filter cavity, thereby achieving a similar response with minimal additional optical components.

The GEO600 detector in Germany [11] is currently the only gravitational wave detector to operate for an extended length of time taking science data using squeezed light to enhance its sensitivity [12,13]. GEO is in a prime position to demonstrate the feasibility of this new technique in the complex setting of a long baseline interferometer. In this paper we take the theory suggested previously for the dual-recycled Fabry-Perot Michelson topology used by LIGO and apply it to GEO, a dual-recycled Michelson without arm cavities. The results in this paper were produced using the numerical interferometer simulation software FINESSE

[14,15], which allowed for the correct modeling of quantum noise behavior taking into account the optical losses of the GEO interferometer.

EPR squeezing was originally proposed to reduce shot noise and radiation pressure noise at the same time. However, the motivation for its use in GEO would be slightly different: the sensitivity of GEO is not currently limited by radiation-pressure noise, as this is masked at low frequencies by technical noises. However, frequency-dependent squeezing would be required for GEO to use squeezing effectively in a detuned mode, in which the signal recycling cavity (SRC) and thus the peak sensitivity of the detector is tuned to a particular offset frequency. This mode of operation has become of interest again with new results suggesting that key information about neutron stars could be obtained from signal frequencies in the kilohertz region in the ringdown phase after a binary merger [16]. We can show that the EPR squeezing technique could be used to operate the GEO detector in such a condition with an effective use of squeezed light to reduce shot noise with sufficient bandwidth at the peak sensitivity at frequencies around 2 kHz. We highlight optical design aspects to be considered for the scheme to be implemented and show how losses ultimately limit the achievable sensitivity improvements. The implementation in GEO600 would not only allow the improvement of its sensitivity, it would also serve as a key technology demonstration for a possible implementation of EPR squeezing in the LIGO detectors.

The structure of this article is as follows: in Sec. II we outline the layout of the GEO detector and how the EPR-squeezing scheme could be implemented. In Sec. III we model how macroscopic length asymmetries between the arms, the *Schnupp asymmetry*, must be carefully chosen for the EPR-squeezing scheme to work. Next, in Sec. IV we look at the squeezing degradation that occurs at the output-mode-cleaners due to an imperfect separation of the signal and idler beams. Finally, in Sec. V we see how optical losses throughout the interferometer also affect the sensitivity.

[*]ddb@star.sr.bham.ac.uk
[†]adf@star.sr.bham.ac.uk

II. SQUEEZING WITH EPR-ENTANGLEMENT IN GEO

To describe the EPR-squeezing scheme we shall first consider the simplified layout shown in Fig. 1 along with the frequency spectrum depicted in Fig. 2. The pair of EPR
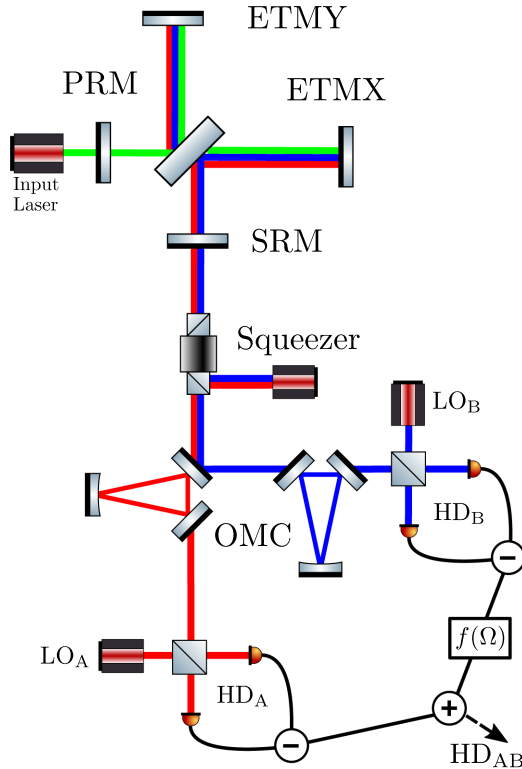

FIG. 1. Simplified optical layout of the GEO600 detector with EPR squeezing. The main carrier light (green) is set to be resonant in the power recycling cavity (PRC). The signal (red) and idler (blue) are injected in the dark port and are resonant within the signal recycling cavity (SRC). On return from the interferometer they are separated and filtered by two output mode cleaner cavities (OMCs).
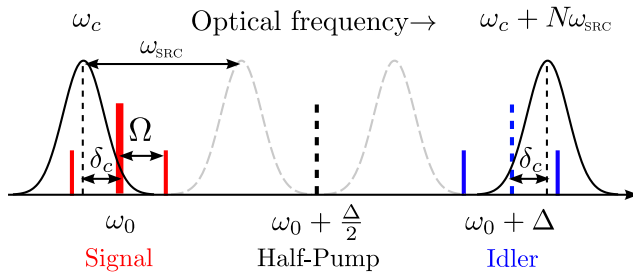

FIG. 2. Sketch showing the frequency components and terms used for describing the EPR-squeezing scheme. ω_c is the optical frequency of a particular FSR of a cavity. The black lines show the signal recycling cavity resonances that the signal and idler fields resonate near, the dashed lines represent the $N-1$ FSRs between them.

entangled beams are generated by an optical parametric amplifier (OPA). The OPA is pumped at a frequency of $2\omega_0 + \Delta$, generating pairs of entangled sidebands around the *signal* (red) frequency ω_0, and the *idler* (blue) frequency $\omega_0 + \Delta$. An incident gravitational wave will generate a pair of sidebands around the signal carrier at frequency $\omega_0 \pm \Omega$. No carrier or signal is present around the idler frequency $\omega_0 + \Delta$. Unlike the typical squeezing injection which entangles light at the frequencies $\omega_0 \pm \Omega$, EPR entanglement correlates fields at $\omega_0 + \Omega$ with fields at $\omega_0 + \Delta - \Omega$ and $\omega_0 - \Omega$ with $\omega_0 + \Delta + \Omega$. This implies the quadratures around ω_0 are correlated with those around $\omega_0 + \Delta$, and thus we can reduce the noise at the signal frequency by making a measurement on the idler—the principal idea behind conditional squeezing.

The signal and idler beams are injected via a Faraday isolator into the output path of the interferometer and enter the interferometer through the signal recycling mirror (SRM). The resonance condition of the dual-recycled interferometer is set so that the main carrier light (green in Fig. 1) destructively interferes going towards the SRM and constructively back towards the power recycling mirror (PRM)—this is known as operating at the *dark fringe*. In this configuration light entering through the SRM is fully reflected back into this port by the interferometer. The SRM and the end test masses, ETMX and ETMY, form the two cavities SRX and SRY. The combination of both of these is referred to as the *signal recycling cavity* (SRC)—a similar argument is made for the PRM, forming PRX, PRY, and the PRC. Table I provides a list of parameter values used in this work for our GEO600 model.

The optical frequency difference between the idler and signal beams, Δ, must be set such that it is close to an integer number of SRC free spectral ranges (FSRs). In particular, with a SRC detuned by a frequency δ_c, the signal and idler frequency difference should be

$$\Delta = N\omega_{\text{SRC}} - 2\delta_c \tag{1}$$

(see Appendix D) for an interferometer free of any defects. In this work we study the effect of EPR squeezing for an

TABLE I. Interferometer parameters used in our GEO600 model.

Parameter	Value
Arm length	1.2 km
Signal-Recycling length	1 m
Power-Recycling length	1.15 m
T_{PRM}	900 ppm
T_{SRM}	0.02
T_{BS}	0.5
T_{ETM}	0
ω_{SRC}	$2\pi \cdot 125$ kHz
ω_{OMC}	$2\pi \cdot 435$ MHz
Input power	2 W

exemplary SRC detuning of 2 kHz including optical losses and asymmetries in the interferometer. The exact value of the frequency is not important for the arguments made here. It was chosen because in principle it allows the improvement of quantum noise unimpeded by other technical noises, and is possibly of interest in the analysis of signals from neutron star mergers.

The detection scheme requires that the signal and idler frequency components are spatially separated and measured individually via balanced homodyne detection. In practice this separation is achieved using a small cavity such as an output mode cleaner (OMC). This cavity must be impedance matched for transmission for one of the signal or idler beams and near antiresonance for maximal reflection of the other. The signals from both homodyne detections are then optimally combined to produce the final output. For this particular GEO600 configuration, with negligible radiation pressure effects, the optimal gain for the signal recombination is frequency independent and depends only on the amount of squeezing present at the output (see Appendix B):

$$K_{\mathrm{opt}} = \pm \tanh(2r), \qquad (2)$$

where r is the squeezing factor. To summarize, four parameters need to be carefully tuned for an optimal readout: the separation frequency Δ, both local oscillator (LO) phases of the homodyne readouts, and the gain factor for the signal recombination. For the interested reader a more mathematical description can be found in Appendices B, C and D of this paper and in the supplemental materials of Ref. [6].

In order to tune the local oscillator phases we start with the homodyne detector measuring the signal beam; in Fig. 1 this is detector HD$_A$. The LO phase must be chosen to optimize the detector's susceptibility to a gravitational wave signal with amplitude h; the transfer function of such a signal to the output HD$_A$ is shown in Fig. 3. The homodyne angle offers a trade-off between high and low frequency susceptibility. In this work we use the 90 deg option as it provides the best broadband response and is similar to the direct current (DC) readout scheme for comparing the EPR scheme against. The numerical value of this angle is of no importance for the EPR aspect of this scheme.

With the required signal homodyne phase being fixed, both Δ and the LO$_B$ homodyne phase must then be optimized. The optimal conditions for these parameters are those that provide the broadest sensitivity around the detuning frequency. This can be achieved by creating a cost function describing the squeezing improvement over the desired frequency range to use with an optimization routine. However, a simpler approach was taken here: it is possible to compute the HD$_{AB}$ output at just the chosen detuning frequency and maximize the relative noise improvement compared to no squeezing injected. In this
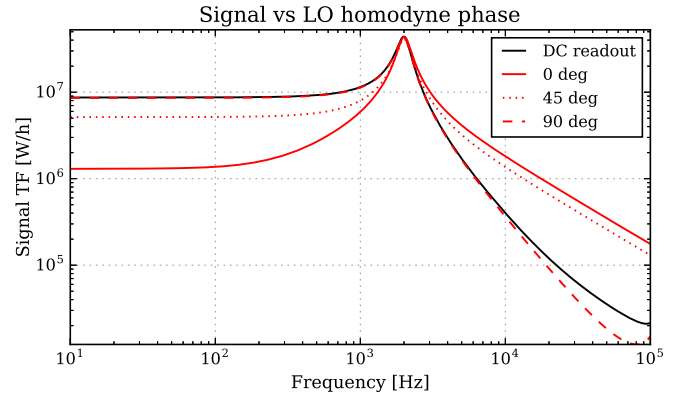

FIG. 3. Signal response of GEO600 with homodyne detection for different homodyne readout angles. This work assumes a 90 deg readout which allows for a direct comparison of the new scheme against the current DC readout scheme.

case we find two optimal points around each of the SRCs FSRs ($\approx$125 kHz). An example of this optimization is shown in Fig. 4 for a detuning of 2 kHz. Here 13 dB of EPR squeezing is injected and $\approx$10 dB of squeezing is seen (see Appendix B on why a 3 dB loss is always present when using EPR squeezing). At 2 kHz above and below the SRC resonance we observe two optimal squeezing conditions. The lower optimal squeezer frequency provides the broadband squeezing required, as specified by Eq. (1), the higher value being the opposite and producing significant
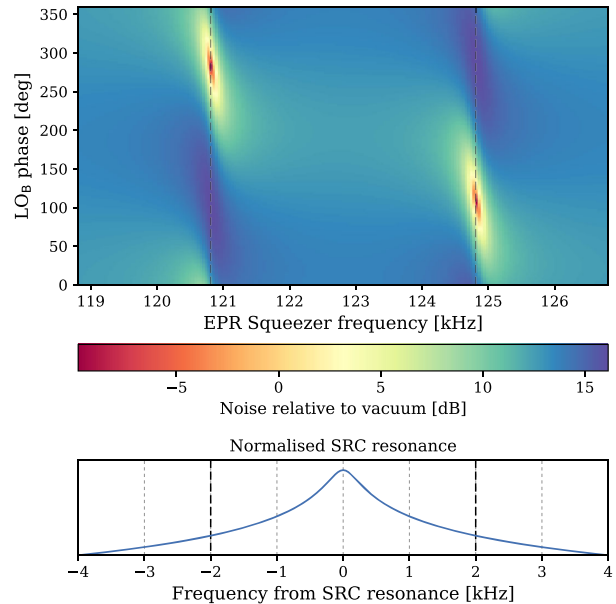

FIG. 4. Optimization for Δ and the LO$_B$ phase for EPR squeezing. The interferometer is detuned at $\delta_c = 2$ kHz. The z-axis of the plot shows the noise output of HD$_{AB}$ at 2 kHz. We find two potential optimal parameters to choose from, the lower frequency one providing the correct broadband noise reduction. The resulting sensitivity of both are shown in Fig. 5.
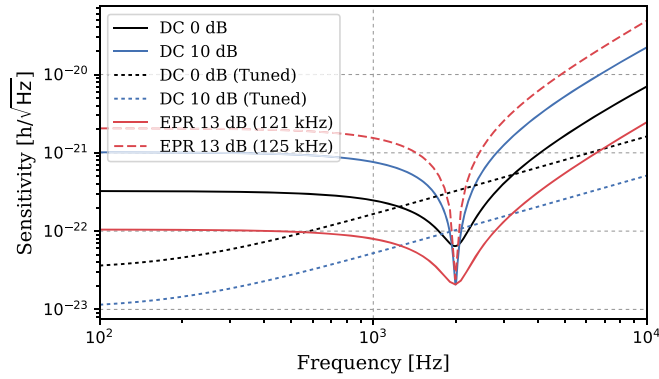
FIG. 5. The standard shot-noise limited sensitivity of the lossless GEO model (both tuned and detuned) is shown in black. For comparison we show that using 10 dB of squeezing with DC readout results in a slight improvement in the detuned case but with significantly narrower bandwidth. The EPR squeezing has two possible parameter choices to optimize the sensitivity at δ_c as shown in Fig. 4, however only one provides the required broadband improvement.

(a) 3cm Schnupp asymmetry

(b) 20cm Schnupp asymmetry

(c) PRM transmission

FIG. 6. The two initial plots illustrate how the choice of the Schnupp asymmetry and the corresponding matching of Δ to $N\omega_{\mathrm{SRC}}$ affects the sensitivity. Using a smaller Schnupp asymmetry reduces the additional resonance peak and results in less distortion near the peak sensitivity. The final plot shows how this additional resonance is affected by the PRM transmission due to the coupling of the SRC and PRC due to a Schnupp asymmetry. The optical power in the arm cavities was kept constant by adjusting the input power in each case to compare this effect.

antisqueezing away from the peak sensitivity. This is analogous to choosing the correct or incorrect squeezing angle using standard squeezing injection with DC readout. Also shown here for reference is the similarly achievable sensitivity when using an equivalent traditional squeezing input of 10 dB with the already used DC readout technique which cannot provide an optimal broadband sensitivity and is only equivalent to a correctly tuned EPR-squeezing scheme at the detuning frequency.

Using a lossless and symmetric GEO model and the optimal parameters found in Fig. 4, the EPR squeezing for both optimal parameter choices are compared to DC readout in Fig. 5. Here we see how an ideal frequency-dependent squeezing scheme can widen the sensitivity around the detuning frequency, below what would normally be achievable in the tuned interferometer case with frequency-independent squeezing. In the following sections we will consider how particular defects affect the performance of the EPR scheme.

III. SCHNUPP ASYMMETRY

Radio frequency (rf) optical modulation is employed in gravitational wave detectors for sensing and control of the position and alignment of optical components. This requires careful design of cavity lengths to ensure that particular frequencies resonate within them. In addition there is a macroscopic differential length difference between the two interferometer arms, known as the *Schnupp asymmetry*. This is required so that, while the main carrier light is still near a dark fringe, some rf sidebands will couple into the output port and thus sense the SRM for control purposes. These rf modulation frequencies are typically of the order of several MHz, thus
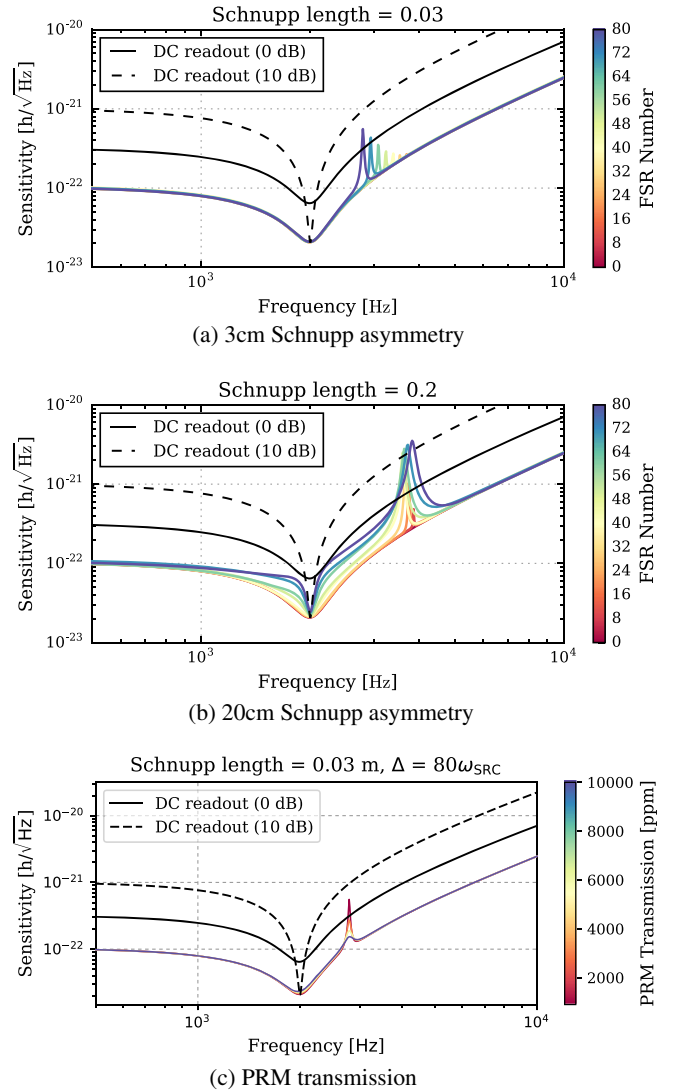
at similar frequencies to that which will be required for the EPR squeezing.

To implement the EPR squeezing scheme the Schnupp asymmetry should be chosen to satisfy design requirements for sensing schemes as well as ensure the higher frequency EPR fields are correctly detuned from an appropriate SRC resonance. To achieve this, the squeezer frequency should be set as an integer number, M, of the Schnupp asymmetry FSR, thus both SRX and SRY are on resonance: $\Delta = Mc/(2L_s)$, where L_s is Schnupp length difference. For technical reasons it is desirable to keep Δ as low as

possible, in the range of tens of MHz, and at a frequency that is well reflected by an OMC. The first value, $M = 1$, for a frequency $\Delta = 2\pi \times 10$ MHz we would require $L_s = 2.4$ m—which begins to be unpractically large.

The second option is to use as small a Schnupp asymmetry as possible instead. Shown in Fig. 6 is how using a Schnupp asymmetry of 3 cm and 20 cm in a simplified GEO model affects the squeezing. The typical feature that appears is an additional resonance peak due to the now different resonant conditions for SRX and SRY and the coupling this generates with the PRC. Appendix A highlights the behavior of these additional peaks in more detail. Figure 6(c) demonstrates how the PRM transmission affects this additional resonance. By lowering the finesse of the PRC we can reduce this feature. However, to achieve similar sensitivities the input power would need to be increased due to the lower PRC recycling gain.

How the sensitivity is affected by the choice of SRC FSR is also shown in Figs. 6(a) and 6(b) up to the 80th FSR—this being equivalent to ≈ 10 MHz. From these figures it is evident that large Schnupp asymmetries quickly degrade the broadband sensitivity as higher SRC FSRs are used. Thus a design requirement for using EPR squeezing is to use the smallest Schnupp asymmetry possible. Currently the asymmetry is set to ≈ 5 cm in GEO which should still allow the benefits of the EPR scheme to be experimentally demonstrated.

IV. SEPARATION OF SIGNAL AND IDLER

So far we have assumed a perfect separation of signal and idler in the detection process. Our models used an OMC with a very narrow linewidth to achieve this. The currently installed OMC at GEO600 has a linewidth of ≈ 1.4 MHz, or $\approx 11\omega_{SRC}$, thus the choice of Δ must be larger than this.

Figure 7 shows the performance of EPR squeezing if we replace the perfect OMC with a realistic model of the OMC. The plot shows the best reduction in noise as a function of Δ in units of ω_{SRC}. With the OMC FSR being

435 MHz, the signal and idler will be ideally separated at ≈ 217.5 MHz $\approx 280\omega_{SRC}$. This large separation is not practical and would require effectively no Schnupp asymmetry. However, reasonable noise reduction is possible up to $80\omega_{SRC}$, showing a reduction in efficiency of about 1 dB compared with an ideal separation of signal and idler.

V. SUSCEPTIBILITY TO OPTICAL LOSSES

Optical losses within an interferometer will degrade any injected squeezed state by introducing uncorrelated pure vacuum noise. For current and future squeezing implementations losses will need to be carefully controlled—for EPR squeezing the loss requirements are more strict. Although in practice losses will occur at each individual optical component, we can classify the losses into three categories: a combined input and output loss, and internal interferometer symmetric and asymmetric losses. To depict how these losses affect the sensitivity, a 2 kHz detuned GEO model was constructed using a Schnupp asymmetry of 5 cm, $\Delta \approx 80$ SRC FSRs, a perfectly separating narrowband OMC, and 13 dB of EPR squeezing. We now compare how three types of loss affects both EPR squeezing and an ideal frequency-dependent squeezing source.

The combined input and output losses refer to any loss on the squeezing input path and those on the output path after the SRM up to the photodiodes. Figure 8 shows how this loss alters the sensitivity of a detector using an ideal frequency-dependent squeezed source (dashed) and with EPR squeezing (solid). Note that a 1% loss here means 1% on input plus another 1% on output. As expected from the work of Ma *et al.* [6], EPR squeezing is approximately twice as sensitive to optical losses compared to conventional frequency-dependent squeezing. Without losses a
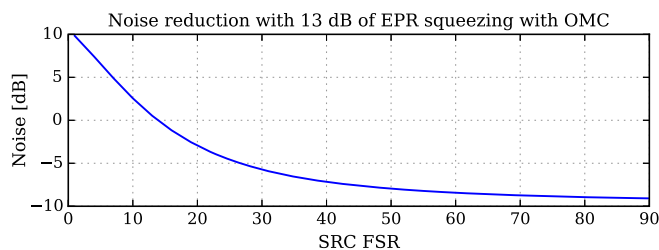

FIG. 7. Noise reduction through EPR squeezing as a function of the frequency Δ given in units of free spectral range (FSR) of the signal recycling cavity (SRC). The current GEO OMC has an linewidth of 1.4 MHz and FSR of 435 MHz. The SRC FSR is 125 kHz. 13 dB of EPR-squeezed light is used to achieve a theoretical maximum noise reduction of 10 dB.
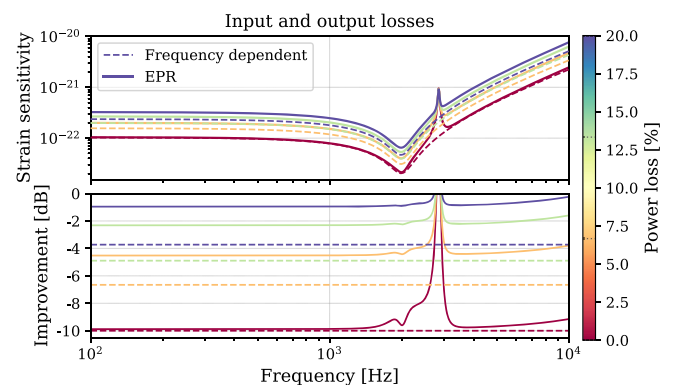

FIG. 8. The effect of losses along the input path and output path on the detector sensitivity for EPR squeezing and for an ideal frequency-dependent squeezed source. Input and output loss of $X\%$ loss refer to an $X\%$ loss on input plus another $X\%$ on output. The lower plot shows the overall improvement of the EPR and ideal squeezing for identical losses. The peak seen here is due to the chosen Schnupp asymmetry.
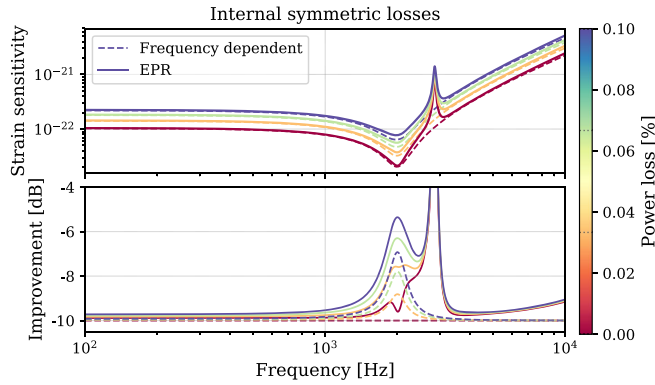
FIG. 9. Effect of internal symmetric losses on the sensitivity of the interferometer. The bottom plot shows the noise reduction achieved by the EPR squeezing and an ideal frequency-dependent source compared to no squeezing in both cases. Significant degradation around the detuning frequency is seen in this case.

10 dB improvement is seen with some degradation around the detuning frequency dip and the additional resonance from the Schnupp asymmetry. A 10% input and output loss results in a reduction to around 3 dB of broadband squeezing. It can also be seen that EPR squeezing degrades faster for a given loss value compared to a perfect frequency-dependent source.

The internal loss in the interferometer such as clipping from finite optics, surface scattering, or absorption can be broken down into either symmetric or asymmetric losses between the two arms. Figure 9 depicts the sensitivity change due to a range of symmetric losses. At the detuning frequency we see the squeezing efficiency is affected by losses to a much greater degree due to the resonance of the signal-recycling cavity multiplying the effect of the loss. Similarly, the asymmetric losses, as shown in Fig. 10, also affect the sensitivity predominantly around the detuning frequency.
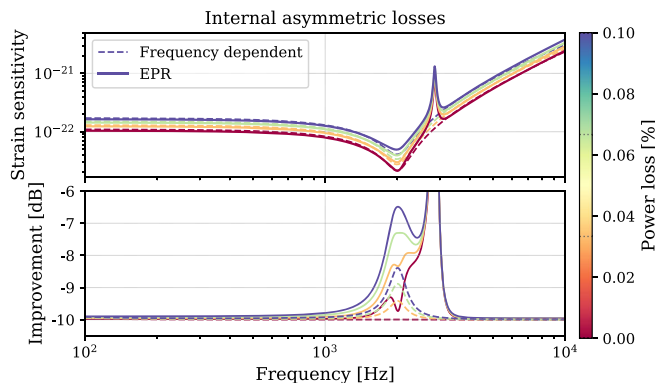

FIG. 10. Effect of asymmetric internal loss in the interferometer on the sensitivity using 10 dB of ideal frequency-dependent squeezing and 13 dB of EPR squeezing. Asymmetric losses adversely affect the sensitivity around the detuning frequency as well as at higher frequencies.

It is instructive to compare our result to current estimates of loss values at GEO600. Internal loss values (symmetric and asymmetric) are estimated to be $\sim 0.1\%$. As we have shown, a loss at this level would result in a substantial reduction in the achievable squeezing around the detuning frequency. The input/output loss is expected to be $\sim 30\%$ in total, which is equivalent to a value around 15% in Fig. 8. Assuming such losses, 13 dB of EPR squeezing could still provide a measurable noise reduction and thus be used for a proof-of-principle demonstration of this technique in a large-scale laser interferometer. However, for operating this scheme in future generations of gravitational wave detectors losses would need to be reduced significantly.

VI. CONCLUSION

We have shown that GEO600 could use the EPR squeezing scheme to improve the shot-noise limited sensitivity with a detuning to 2 kHz without reducing the detector bandwidth. We have considered the frequency separation of the signal and idler beams to be in the MHz range for practical reasons. This in turn leads to the requirement that the Schnupp asymmetry must be kept as small as possible to suppress additional optical resonances and to provide the best broadband noise reduction. A Schnupp asymmetry of ≈ 3 cm would be sufficient according to our results. The best value for the Schnupp asymmetry should be based on a trade-off between this effect and the transmission of the optical rf sidebands required for controlling the interferometer.

We have shown how the separation of signal and idler by a realistic OMC slightly reduces the efficiency of the scheme: the reduction of effective squeezing at around $\Delta \approx 80\omega_{\mathrm{SRC}} \approx 2\pi \times 10$ MHz using the cavity parameters for the current GEO OMC (excluding its losses) has been shown to be around 1 dB.

Optical losses are limiting the effectiveness of all quantum noise reduction techniques. We have demonstrated how the sensitivity of GEO600 with EPR squeezing is affected by losses in the input and output path, and by losses inside the interferometer. These results can be used to derive requirements for potential upgrades for reducing current optical losses to a level that render the implementation of EPR squeezing feasible.

Overall we found no theoretical design aspects that would significantly hinder the application of EPR squeezing in GEO. The current loss estimates within GEO600 suggest that EPR squeezing would offer minimal benefits to the overall sensitivity of the detector without an addition reduction of the optical losses. However, GEO600 could provide an important experimental verification in an active detector of this technique which is considered an interesting alternative to the conventional approach of using filter cavities for detector upgrades and in future detector designs.

APPENDIX A: PEAK BEHAVIOR PRC-SRC SCHNUPP COUPLING

By introducing a coupling between the PRC and SRC, additional peaks appear in the sensitivity spectrum, as shown in Fig. 6. There are two regimes to consider: the weak [Fig. 6(a)] and strong [Fig. 6(b)] coupled cases. When a coupled cavity becomes strongly coupled an additional resonance is present. We can see this in Fig. 11. This shows the power build up in the PRC-SRC coupled cavity due to a 1 W optical field injected at the dark port for a range of asymmetries. This is injected at a frequency $\sim 80\omega_{SRC}$ to model how the idler fields respond to a coupled system. For the signal fields this coupling is negligibly small and only a single resonance is seen.

With the idler sidebands seeing a different optical response from the signal sidebands the optimal sensitivity achievable is degraded as seen in the previous sections. In Fig. 11 we see for small Schnupp asymmetries the PRC power is lower and the SRC is a single peak. As the asymmetries are increased the PRC power is of the order or greater than that in the SRC and the two become strongly coupled. From here an additional resonance is visible which further separates in frequency space as the coupling strength increases.

In Fig. 6 we see the new resonance beginning to appear around 4 kHz. This is determined by the choice of δ_c. The idler is offset from the SRC resonance by $-\delta_c$ and the PRC resonance is $+\delta_c$. Thus at $2\delta_c$ the idler's upper sideband resonates in the PRC when coupling between the SRC and PRC is present.

In Fig. 6 this new resonance drift shifts in frequency depending on the asymmetry and chosen Δ. The broadband squeezing is achieved by correctly rotating the squeezed state, which is determined by the relative phase between the upper and lower signal and idler sidebands accumulated on reflection from a cavity (see Eq. (D5). When determining the idler's carrier frequency value by optimizing Δ, the lower frequency SRC peak is found to provide the best

(a) PRC power response

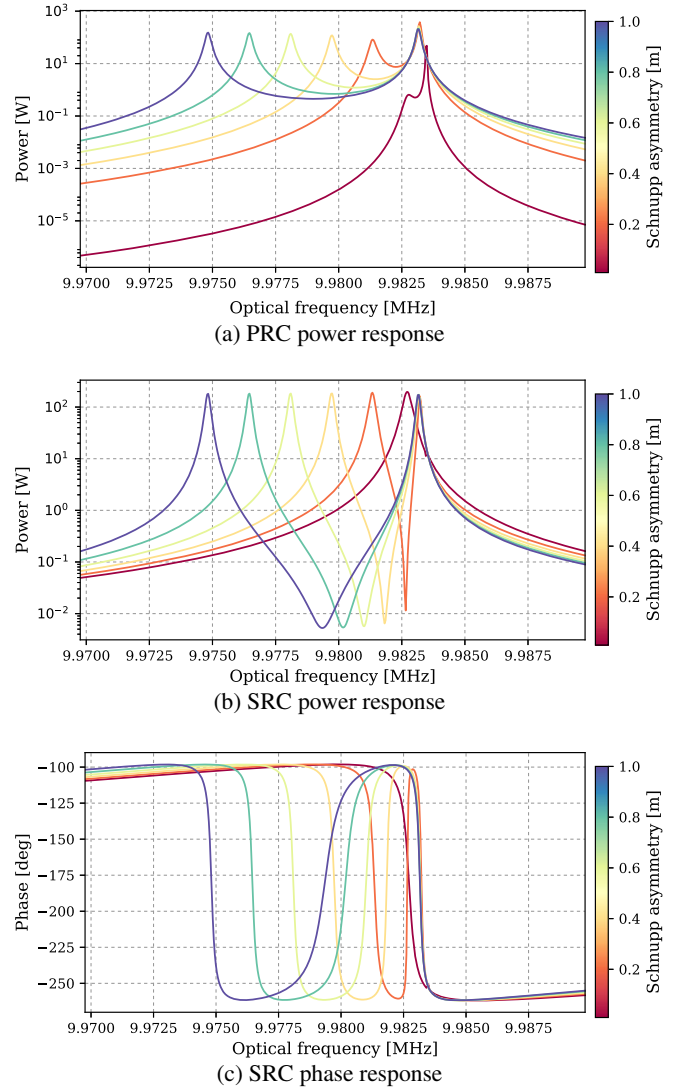(b) SRC power response

(c) SRC phase response

FIG. 11. Shown are the powers in the PRC and SRC due to a single frequency optical field injected at the dark port. Figure 11(c) shows the phase of the field in the SRC. This field's frequency is swept over a similar range to what the idler sidebands would be for $\Delta \approx 80\omega_{SRC}$, to visualize how they will react to a weak or strongly coupled cavity due to asymmetries. The sharper features seen are from the PRC resonance due to its higher finesse. As the asymmetric coupling is increased the PRC and SRC become strongly coupled and a split resonance is seen. The new resonances also alter the phase of the sidebands in the SRC affecting the correct squeezing angle rotation.

broadband noise reduction. Using the lower peak means that the upper idler sideband then interacts with the resonance conditions that appear. Figure 11(c) depicts the phase of an optical field reflected from the SRC over the frequency range of the idler sidebands. We can see there is a fast change in phase of the sideband around the SRC resonance. The new resonance, from the strongly coupled cavities, introduces a second phase jump resulting in an incorrect rotation of the squeezed state at particular

frequencies. This is the reason for the additional peaks in Fig. 6.

APPENDIX B: ENTANGLEMENT AT A BEAM SPLITTER

As shown in Fig. 12, we denote the incoming entangled fields from the west port of the beam splitter as $\hat{c}$ and the south port as $\hat{d}$, and the outgoing field to the north port as $\hat{a}$ and east port as $\hat{b}$. They satisfy the following input-output relation:

$$\hat{a} = \frac{1}{\sqrt{2}}(\hat{c} + \hat{d}), \qquad \hat{b} = \frac{1}{\sqrt{2}}(\hat{c} - \hat{d}). \quad (B1)$$

In terms of the amplitude quadrature $\hat{o}_1 = (\hat{o} + \hat{o}^\dagger)/\sqrt{2}$ and phase quadrature $\hat{o}_2 = (\hat{o} + \hat{o}^\dagger)/(\sqrt{2}i)$, the above input-output relation can be rewritten as

$$\begin{bmatrix} \hat{a}_1 \\ \hat{a}_2 \\ \hat{b}_1 \\ \hat{b}_2 \end{bmatrix} = \frac{1}{\sqrt{2}} \begin{bmatrix} 1 & 0 & 1 & 0 \\ 0 & 1 & 0 & 1 \\ 1 & 0 & -1 & 0 \\ 0 & 1 & 0 & -1 \end{bmatrix} \begin{bmatrix} \hat{c}_1 \\ \hat{c}_2 \\ \hat{d}_1 \\ \hat{d}_2 \end{bmatrix}. \quad (B2)$$

The covariance matrix of the ingoing field is defined as

$$\mathbf{V}_{\text{in}} = \langle \psi | \begin{bmatrix} \hat{c}_1 \\ \hat{c}_2 \\ \hat{d}_1 \\ \hat{d}_2 \end{bmatrix} [\hat{c}_1 \quad \hat{c}_2 \quad \hat{d}_1 \quad \hat{d}_2] | \psi \rangle \quad (B3)$$

with $|\psi\rangle$ being the quantum state of the optical field. Assuming that $\hat{c}$ is amplitude squeezed and $\hat{d}$ is phase squeezed (illustrated by the noise ellipse in Fig. 12) we have

$$\mathbf{V}_{\text{in}} = \begin{bmatrix} e^{-2r} & 0 & 0 & 0 \\ 0 & e^{2r} & 0 & 0 \\ 0 & 0 & e^{2r} & 0 \\ 0 & 0 & 0 & e^{-2r} \end{bmatrix}, \quad (B4)$$

in which r is the squeezing factor. The resulting covariance matrix $\mathbf{V}_{\text{out}}$ for the outgoing field, using the input-output relation Eq. (B2), is then

$$\mathbf{V}_{\text{out}} = \begin{bmatrix} \cosh 2r & 0 & -\sinh 2r & 0 \\ 0 & \cosh 2r & 0 & \sinh 2r \\ -\sinh 2r & 0 & \cosh 2r & 0 \\ 0 & \sinh 2r & 0 & \cosh 2r \end{bmatrix}. \quad (B5)$$

We can see from this that the amplitude quadrature and phase quadrature for either the outgoing field $\hat{a}$ or $\hat{b}$ are not
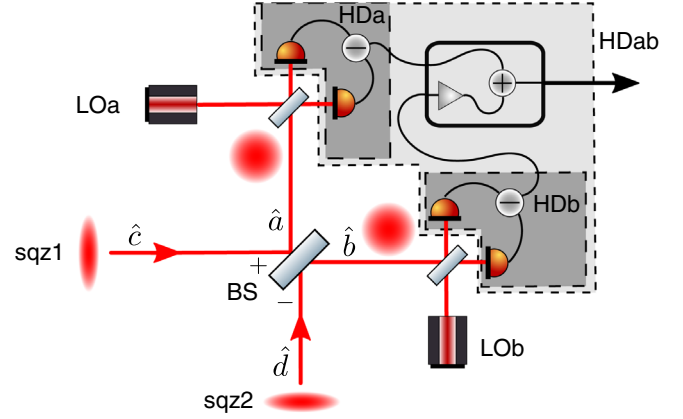

FIG. 12. Entanglement through overlapping two squeezed fields.

correlated, which is illustrated schematically by using a noise circle in Fig. 12. However, $\hat{a}$ and $\hat{b}$ are mutually correlated, or equivalently forming a quantum entanglement, manifested by the nonzero off-diagonal terms in the covariance matrix $\mathbf{V}_{\text{out}}$. It is such a correlation that allows us to reduce the uncertainty (variance) of $\hat{a}$ by making a measurement on $\hat{b}$, or vice versa. This is the main principle behind the *conditional squeezing*.

Suppose HD_A measures

$$\hat{a}_\theta \equiv \hat{a}_1 \sin \theta + \hat{a}_2 \cos \theta \quad (B6)$$

and HD_B measures

$$\hat{b}_\phi \equiv \hat{b}_1 \sin \phi + \hat{b}_2 \cos \phi. \quad (B7)$$

We construct the following estimator for $\hat{a}_\theta$ using the measurement outcome of $\hat{b}_\phi$:

$$\hat{a}_\theta^{\text{est}} \equiv K\hat{b}_\phi, \quad (B8)$$

in which K is some coefficient (filter function). The conditional variance of $\hat{a}_\theta$ is defined as

$$\begin{aligned} V_{a_\theta a_\theta}^{\text{cond}} &\equiv \min_K \langle \psi | (\hat{a}_\theta - \hat{a}_\theta^{\text{est}})^2 | \psi \rangle \\ &= \min_K [V_{a_\theta a_\theta} - 2KV_{a_\theta b_\phi} + K^2 V_{b_\phi b_\phi}] \\ &= \min_K \left[V_{a_\theta a_\theta} - \frac{V_{a_\theta b_\phi}^2}{V_{b_\phi b_\phi}} + V_{b_\phi b_\phi} \left(K - \frac{V_{a_\theta b_\phi}}{V_{b_\phi b_\phi}} \right)^2 \right]. \end{aligned}$$
$$(B9)$$

The optimal value for K (Wiener filter) is given by

$$K_{\text{opt}} = \frac{V_{a_\theta b_\phi}}{V_{b_\phi b_\phi}}. \tag{B10}$$

Given the covariance matrix $\mathbf{V}_{\text{out}}$ shown in Eq. (B5) for the outgoing field, we have

$$V_{a_\theta a_\theta}^{\text{cond}} = \cosh 2r - \cos^2(\theta + \phi)\sinh 2r \tanh 2r \tag{B11}$$

and

$$K_{\text{opt}} = \cos(\theta + \phi)\tanh 2r. \tag{B12}$$

Therefore, to get the minimum conditional variance for $\hat{a}_\theta$, we need to measure the proper $\hat{b}_\phi$ such that

$$\phi = -\theta, \quad \text{or} \quad \phi = \pm\pi - \theta. \tag{B13}$$

which yields

$$V_{a_\theta a_\theta}^{\text{cond}}\big|_{\min} = \cosh 2r - \sinh 2r \tanh 2r = \frac{1}{\cosh 2r}, \tag{B14}$$

and

$$K_{\text{opt}} = \pm\tanh 2r, \tag{B15}$$

in which the sign depends on the choice of ϕ in Eq. (B13). This is the optimal gain factor to use when combining the signal and idler beams. Note that this is a frequency independent factor, which is not the case when radiation pressure effects are dominant. In particular, given 10 dB input squeezing for both $\hat{c}$ and $\hat{d}$, the observed conditional squeezing is approximately equal to 7 dB, i.e.,

$$10\log_{10}(e^{2r}) = 10 \to 10\log_{10}(\cosh 2r) \approx 7, \tag{B16}$$

or that the EPR squeezing scheme results in an automatic 3 dB loss in squeezing.

APPENDIX C: ENTANGLEMENT IN THE SQUEEZER

Here we analyze the case of entanglement (correlation) generated from a squeezer with a squeezing spectrum over a wide frequency range (usually up to 100 MHz). The various relevant frequencies for the fields are illustrated in Fig. 13. In particular, $\omega_0 + \Delta/2$ is half of the pump frequency of the squeezer. For the usual squeezing injection in the gravitational-wave detector, this frequency normally coincides with the main carrier frequency. However, in the EPR squeezing scheme, it is intentionally offset from the carrier at ω_0 by $\Delta/2$ with Δ of the order of MHz. As a result, the sidebands around ω_0 and those around $\omega_0 + \Delta$ are correlated. Specifically, the optical field $\hat{o}(\omega_0 - \Omega)$ is correlated with $\hat{o}(\omega_0 + \Delta + \Omega)$, and $\hat{o}(\omega_0 + \Omega)$ is correlated with $\hat{o}(\omega_0 + \Delta - \Omega)$. To distinguish between the
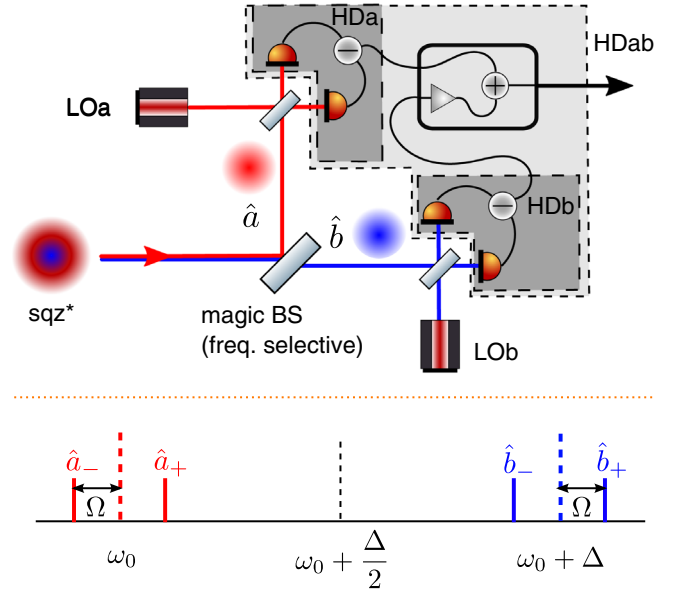

FIG. 13. Entangled squeezed input and *magic beam splitter*. In practice this frequency dependent splitting is achieved through an optical cavity, reflecting one frequency and transmitting another.

sidebands around ω_0 and those around $\omega_0 + \Delta$, we introduce

$$\hat{a}_\pm \equiv \hat{o}(\omega_0 \pm \Omega), \qquad \hat{b}_\pm \equiv \hat{o}(\omega_0 + \Delta \pm \Omega). \tag{C1}$$

Given the frequency-independent squeezing source with squeezing factor r and angle θ_s ($\theta_s = 0$ corresponds to phase squeezing), their correlations can be described by using spectral density, and we have

$$S_{a_+ a_+} = S_{a_- a_-} = S_{b_+ b_+} = S_{b_- b_-} = \cosh 2r, \tag{C2}$$

$$S_{b_- a_+} = S_{a_+ b_-}^* = S_{b_+ a_-} = S_{a_- b_+}^* = e^{2i\theta_s}\sinh 2r, \tag{C3}$$

$$S_{a_- a_+} = S_{a_- b_-} = S_{a_+ b_+} = S_{b_- b_+} = 0, \tag{C4}$$

where the single-sided spectral density S_{AB} is defined through

$$\frac{1}{2\pi}\langle\psi|\hat{A}(\Omega)\hat{B}^\dagger(\Omega') + \hat{B}^\dagger(\Omega')\hat{A}(\Omega)|\psi\rangle \equiv S_{AB}(\Omega)\delta(\Omega - \Omega'). \tag{C5}$$

With Eqs. (C2), (C3), and (C4), we can derive the covariance matrix for $[\hat{a}_1 \hat{a}_2 \hat{b}_1 \hat{b}_2]$, in terms of spectral density, as

$$\mathbf{S} = \begin{bmatrix} S_{a_1 a_1} & S_{a_1 a_2} & S_{a_1 b_1} & S_{a_1 b_2} \\ S_{a_2 a_1} & S_{a_2 a_2} & S_{a_2 b_1} & S_{a_2 b_2} \\ S_{b_1 a_1} & S_{b_1 a_2} & S_{b_1 b_1} & S_{b_1 b_2} \\ S_{b_2 a_1} & S_{b_2 a_2} & S_{b_2 b_1} & S_{b_2 b_2} \end{bmatrix} = \begin{bmatrix} \cosh 2r & 0 & \cos 2\theta_s \sinh 2r & \sin 2\theta_s \sinh 2r \\ 0 & \cosh 2r & \sin 2\theta_s \sinh 2r & -\cos 2\theta_s \sinh 2r \\ \cos 2\theta_s \sinh 2r & \sin 2\theta_s \sinh 2r & \cosh 2r & 0 \\ \sin 2\theta_s \sinh 2r & -\cos 2\theta_s \sinh 2r & 0 & \cosh 2r \end{bmatrix}. \quad (C6)$$

In the special case when $\theta_s = \pi/2$ (amplitude squeezing injection), the above covariance matrix becomes identical to Eq. (B5), i.e.,

$$\mathbf{S}|_{\theta_s = \pi/2} = \begin{bmatrix} \cosh 2r & 0 & -\sinh 2r & 0 \\ 0 & \cosh 2r & 0 & \sinh 2r \\ -\sinh 2r & 0 & \cosh 2r & 0 \\ 0 & \sinh 2r & 0 & \cosh 2r \end{bmatrix}. \quad (C7)$$

Even though the generation of entanglement is different from the previous example shown in Fig. 12, the resulting structure of entanglement is almost the same, when looking at each frequency. Therefore, the reduction of uncertainty in $\hat{a}$, i.e., the conditional squeezing, by the measurement of $\hat{b}$ follows the same logic as we previously discussed.

APPENDIX D: APPENDIX D: ENTANGLED SQUEEZING AND FREQUENCY INDEPENDENT RECOMBINATION WITH A SIMPLE DETUNED CAVITY

We now look at the effect of the optical cavity on the squeezing field, as shown schematically in Fig. 14. This optical cavity in theory represents the SRC of GEO600. In the sideband picture, the input-output relation is given by

$$\hat{o}_{\text{out}}(\omega) = -\frac{\omega - \omega_c - i\gamma_c}{\omega - \omega_c + i\gamma_c}\hat{o}_{\text{in}}(\omega), \quad (D1)$$

where ω_c is the cavity resonant frequency, and γ_c is the cavity bandwidth.

Take the sideband fields $\hat{a}_\pm = \hat{o}(\omega_0 \pm \Omega)$ for example:

$$\hat{a}_{\text{out}\pm} = -\frac{\pm\Omega + \delta_c - i\gamma_c}{\pm\Omega + \delta_c + i\gamma_c}\hat{a}_{\text{in}\pm} \equiv e^{i\phi_\pm}\hat{a}_{\text{in}\pm}, \quad (D2)$$

where we have introduced cavity detuning δ_c and sideband phase $\phi_\pm$:

$$\delta_c \equiv \omega_0 - \omega_c, \qquad \phi_\pm \equiv 2\arctan\left(\frac{\pm\Omega + \delta_c}{\gamma_c}\right). \quad (D3)$$

In the quadrature picture, the above input-output relation can be rewritten as

$$\begin{bmatrix} \hat{a}_{\text{out}1} \\ \hat{a}_{\text{out}2} \end{bmatrix} = e^{i(\frac{\phi_+ - \phi_-}{2})}\begin{bmatrix} \cos\frac{\phi_+ + \phi_-}{2} & -\sin\frac{\phi_+ + \phi_-}{2} \\ \sin\frac{\phi_+ + \phi_-}{2} & \cos\frac{\phi_+ + \phi_-}{2} \end{bmatrix}\begin{bmatrix} \hat{a}_{\text{in}1} \\ \hat{a}_{\text{in}2} \end{bmatrix}. \quad (D4)$$

A similar relation can also be established between $\hat{b}_{\text{out}1,\text{out}2}$ and $\hat{b}_{\text{in}1,\text{in}2}$. As we can see, the quadrature is rotated by a frequency-dependent angle equal to

$$\frac{\phi_+ + \phi_-}{2} = \arctan\left(\frac{\Omega + \delta_c}{\gamma_c}\right) + \arctan\left(\frac{-\Omega + \delta_c}{\gamma_c}\right). \quad (D5)$$

When the cavity detuning changes sign, the rotation angle also changes sign correspondingly, namely,

$$\frac{\phi_+ + \phi_-}{2}\bigg|_{\delta_c \to -\delta_c} = -\left(\frac{\phi_+ + \phi_-}{2}\right). \quad (D6)$$
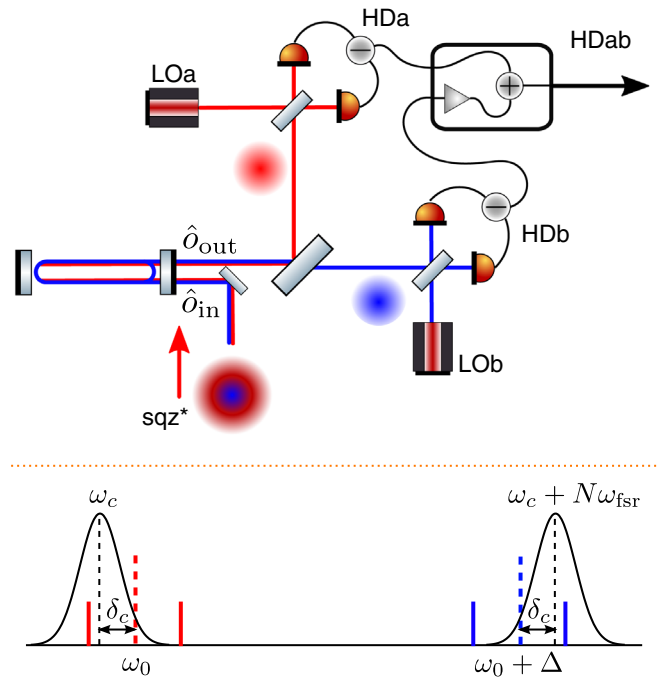

FIG. 14. An entangled squeezed input reflected from a cavity can provide a frequency independent squeezing when recombined.

Therefore if we arrange the frequency in a way as illustrated in Fig. 14—ω_0 is blue detuned with respect to ω_c while $\omega_0 + \Delta$ is red detuned with respect to $\omega_c + N\omega_{\mathrm{fsr}}$ with ω_{fsr} being the free spectral range of the cavity, $\hat{a}_{\mathrm{in1,in2}}$ will be rotated opposite to $\hat{b}_{\mathrm{in1,in2}}$. From Eq. (B13), this will ensure that the conditional squeezing achieves the minimum level at all frequencies, as seen in the main results of the paper.

[1] C. M. Caves, Quantum-mechanical noise in an interferometer, Phys. Rev. D **23**, 1693 (1981).

[2] R. Schnabel, N. Mavalvala, D. E. McClelland, and P. K. Lam, Quantum metrology for gravitational wave astronomy, Nat. Commun. **1**, 121 (2010).

[3] E. Oelker, T. Isogai, J. Miller, M. Tse, L. Barsotti, N. Mavalvala, and M. Evans, Audio-Band Frequency-Dependent Squeezing for Gravitational-Wave Detectors, Phys. Rev. Lett. **116**, 041102 (2016).

[4] M. Evans, L. Barsotti, P. Kwee, J. Harms, and H. Miao, Realistic filter cavities for advanced gravitational wave detectors, Phys. Rev. D **88**, 022002 (2013).

[5] P. Kwee, J. Miller, T. Isogai, L. Barsotti, and M. Evans, Decoherence and degradation of squeezed states in quantum filter cavities, Phys. Rev. D **90**, 062006 (2014).

[6] Y. Ma, H. Miao, B. H. Pang, M. Evans, C. Zhao, J. Harms, R. Schnabel, and Y. Chen, Proposal for gravitational-wave detection beyond the standard quantum limit through EPR entanglement, Nat. Phys. **13**, 776 (2017).

[7] M. D. Reid, Demonstration of the Einstein-Podolsky-Rosen paradox using nondegenerate parametric amplification, Phys. Rev. A **40**, 913 (1989).

[8] B. Hage, A. Samblowski, and R. Schnabel, Towards Einstein-Podolsky-Rosen quantum channel multiplexing, Phys. Rev. A **81**, 062301 (2010).

[9] J. Zhang, Einstein-Podolsky-Rosen sideband entanglement in broadband squeezed light, Phys. Rev. A **67**, 054302 (2003).

[10] A. Einstein, B. Podolsky, and N. Rosen, Can quantum-mechanical description of physical reality be considered complete?, Phys. Rev. **47**, 777 (1935).

[11] K. L. Dooley and LIGO Scientific Collaboration, Status of GEO600, J. Phys. Conf. Ser. **610**, 012015 (2015).

[12] J. Abadie *et al.* (LIGO Scientific Collaboration), A gravitational wave observatory operating beyond the quantum shot-noise limit: Squeezed light in application, Nat. Phys. **7**, 962 (2011).

[13] C. Affeldt *et al.*, Advanced techniques in GEO600, Classical Quantum Gravity **31**, 224002 (2014).

[14] A. Freise, G. Heinzel, H. Lück, R. Schilling, B. Willke, and K. Danzmann, Frequency-domain interferometer simulation with higher-order spatial modes, Classical Quantum Gravity **21**, S1067 (2004); Finesse is available at http://www.gwoptics.org/finesse.

[15] D. D. Brown, Interaction of light and mirrors: Advanced techniques for modeling future gravitational wave detectors, Ph.D. thesis, University of Birmingham, 2015.

[16] L. Rezzolla and K. Takami, Gravitational-wave signal from binary neutron stars: A systematic analysis of the spectral properties, Phys. Rev. D **93**, 124051 (2016).